J|A|C|S ARTICLES

Published on Web 04/30/2010

# Pseudocapacitive Contributions to Charge Storage in Highly Ordered Mesoporous Group V Transition Metal Oxides with Iso-Oriented Layered Nanocrystalline Domains

Kirstin Brezesinski,[†] John Wang,[‡,#] Jan Haetge,[†] Christian Reitz,[†] Sven O. Steinmueller,[†] Sarah H. Tolbert,[§,||] Bernd M. Smarsly,[†] Bruce Dunn,[‡,||] and Torsten Brezesinski*[,†]

*Institute of Physical Chemistry, Justus-Liebig-University Giessen, Heinrich-Buff-Ring 58, 35392 Giessen, Germany, Department of Materials Science and Engineering, University of California, Los Angeles, California 90095-1595, Department of Chemistry and Biochemistry, University of California, Los Angeles, California 90095-1569, and The California NanoSystems Institute, University of California, Los Angeles, California 90095*

Received December 23, 2009; E-mail: torsten.brezesinski@phys.chemie.uni-giessen.de

***Abstract:*** Amphiphilic block copolymers are very attractive as templates to produce inorganic architectures with nanoscale periodicity because of their ability to form soft superstructures and to interact with inorganic materials. In this paper, we report the synthesis and electrochemical properties of highly ordered mesoporous *T*-$Nb_2O_5$, *L*-$Ta_2O_5$, and $TaNbO_5$ solid solution thin films with iso-oriented layered nanocrystalline domains. These oxide materials were fabricated by coassembly of inorganic sol−gel reagents with a poly(ethylene-*co*-butylene)-*b*-poly(ethylene oxide) diblock copolymer, referred to as KLE. We establish that all materials employed here are highly crystalline and have an ordered cubic pore-solid architecture after thermal treatment. We also demonstrate that these group V transition metal oxides can be readily produced with a high degree of crystallographic alignment on virtually any substrate in contrast to classical solution-phase epitaxy which requires the use of a single-crystalline substrate to achieve oriented crystal growth. Moreover, we show the benefits of producing a material with both a mesoporous morphology and crystallographically oriented domains. Mesoporous *T*-$Nb_2O_5$ films exhibit high levels of pseudocapacitive charge storage and much higher capacities than mesoporous amorphous films of the same initial $Nb_2O_5$ composition. Part of this high capacity stems from very facile intercalation pseudocapacitance. This process occurs at rates comparable to traditional redox pseudocapacitance in high surface area $Nb_2O_5$ because of the periodic nanoscale porosity, the iso-orientation of the layered nanocrystalline pore walls, and the mechanical flexibility of periodic porous materials.

## Introduction

In recent years, it has been shown that polymer templating of inorganic materials can be used to prepare nanostructured inorganic−organic composites.[1−3] The formation of these materials relies on the solution phase coassembly of inorganic reagents with organic structure-directing agents to produce long-range periodicities. Once the inorganic material is fully cross-linked, the organic template can be removed by either thermal treatment or solvent extraction to produce periodic pore-solid architectures. Because of the high degree of chemical control available, the pore-to-pore distance, inorganic wall thickness, and pore symmetry as well as orientation can be varied independently. The corresponding thin film materials can be produced by the same coassembly methods but using an evaporation-induced self-assembly (EISA) process.[4−6]

Although a significant number of research reports reflect the enthusiasm and strong conviction concerning the general applicability of sol−gel type mesoporous metal oxide films, only limited progress has been made in using such materials for sensing, energy storage, etc. To some degree, this limitation is the result of diverse engineering-related issues that need to be solved for such applications to become viable. However, it is apparent that there are some fundamental issues that need to be overcome to meet the stringent requirements imposed by various applications. For example, well-defined porosity, high crystallinity, and thermal stability are a prerequisite for many

[†] Justus-Liebig-University Giessen.
[‡] Department of Materials Science and Engineering, University of California at Los Angeles.
[§] Department of Chemistry and Biochemistry, University of California at Los Angeles.
[||] The California NanoSystems Institute, University of California at Los Angeles.
[#] Present address: HRL Laboratories, LLC, Malibu, CA 90265.

(1) Beck, J. S.; Vartuli, J. C.; Roth, W. J.; Leonowicz, M. E.; Kresge, C. T.; Schmitt, K. D.; Chu, C. T. W.; Olson, D. H.; Sheppard, E. W.; McCullen, S. B.; Higgins, J. B.; Schlenker, J. L. *J. Am. Chem. Soc.* **1992**, *114*, 10834–10843.
(2) Mann, S. *Nat. Mater.* **2009**, *8*, 781–792.
(3) Goltner, C. G.; Antonietti, M. *Adv. Mater.* **1997**, *9*, 431–436.
(4) Brinker, C. J.; Lu, Y. F.; Sellinger, A.; Fan, H. Y. *Adv. Mater.* **1999**, *11*, 579–585.
(5) Richman, E. K.; Brezesinski, T.; Tolbert, S. H. *Nat. Mater.* **2008**, *7*, 712–717.
(6) Ogawa, M. *Langmuir* **1997**, *13*, 1853–1855.

 **10.1021/ja9106385** 

applications.[7,8] The synthesis of materials that combine those key features, however, still constitutes a major challenge to current templating routes.

Hierarchical pore architectures have provided a convenient route for achieving more complexity/functionality in thin film materials.[9−11] However, one factor which has been largely neglected is control of the crystallization process. While the importance of a high degree of crystallinity has been pointed out frequently, much less attention has been devoted to the crystallographic orientation of crystalline domains in the inorganic wall structure.[12−15] Nanocrystalline grain structures typically show a random orientation with respect to both substrate and mesopore structure. The lack of control over crystallographic orientation thus constitutes a limitation of sol−gel type mesoporous oxide films, as different crystallographic faces can lead to distinctly different physical and chemical properties. Although the oriented attachment of nanocrystals has proven to be a promising approach to produce one-dimensional nanostructures, at present, there is no indication of how one might align such particles on an arbitrary substrate.[16,17] It would seem that one appropriate route to obtaining thin films with highly oriented nanocrystalline pore walls is through the use of molecular precursors, as there is the prospect of converting the initially amorphous framework to achieve unidirectional nucleation.

Recently, we have introduced the concept of "soft epitaxy" to describe the result that polymer-templated molybdenum oxide ($MoO_3$) films exhibit iso-oriented layered nanocrystalline domains after thermal treatment.[18,19] In that work, the basic requirement for preferred crystallographic orientation appeared to be highly anisotropic bonding. We showed that the anisotropic distribution of atoms in the orthorhombic unit cell of molybdite ($\alpha$-$MoO_3$) allows for the production of films with crystallographically oriented nanocrystals, and demonstrated further that the iso-orientation has, in fact, a profound effect on the charge storage properties of $\alpha$-$MoO_3$.[19]

The present work proves the generality of our previous $MoO_3$ results and specifically focuses on niobium oxide ($Nb_2O_5$) and tantalum oxide ($Ta_2O_5$), materials that we show can also be synthesized with periodic nanoscale porosity and crystallographically oriented nanocrystalline walls. $\alpha$-$MoO_3$ has been shown to be a very interesting material for electrochemical energy storage, and we demonstrate here that ordered mesoporous *T*-$Nb_2O_5$ with a layered crystalline wall structure also possesses considerable potential as an electrode material for electrochemical capacitor applications.[19]

Currently, there is widespread interest in using pseudocapacitor-based materials for electrochemical capacitors because the energy density associated with faradaic reactions is substantially larger, by at least 1 order of magnitude, than electric double layer capacitors. The latter is largely associated with carbon-based materials.[20,21] We note that Sanchez et al. showed recently that mesoporous hydrated $RuO_2$ films can deliver up to 1000 F/g; however, the high price of ruthenium makes such capacitive storage devices unsuitable for widespread applications.[22] Our previous results with iso-oriented $\alpha$-$MoO_3$ showed that significant enhancement in pseudocapacitance was achieved because of the unique combination of nanoscale porosity and oriented nanocrystalline domains with van der Waals gaps.[19] Here, we confirm this conclusion by showing similarly impressive electrochemical performance in a chemically unrelated material that has the same nanoscale architecture and a comparable iso-oriented domain structure.

In this work, we examine the preparation of ordered mesoporous *T*-$Nb_2O_5$ and *L*-$Ta_2O_5$ as well as of mixed $TaNbO_5$ films and explore the electrochemical properties of $Nb_2O_5$. We show that the initially amorphous frameworks can be fully crystallized while retaining nanoscale order by moving to a templated structure with sufficiently thick pore walls. We further show that all three oxides can be readily produced with a high degree of crystallographic orientation on virtually any substrate by soft solution-processing routes. The purpose of this manuscript, however, is not to be just another example of a mesoporous material. Instead, the goal was to unravel further features of "soft epitaxy" to validate the general design rules developed using $\alpha$-$MoO_3$ as a nanoscale structural route for achieving enhanced pseudocapacitance in a single material.[19]

***Table 1.*** Recipes for the Synthesis of Sol-Gel Type $Nb_2O_5$, $Ta_2O_5$, and $TaNbO_5$ Solid Solution Thin Films

| | $NbCl_5$ (mg) | $Ta(OC_2H_5)_5$ (mg) | KLE (mg) | $H_2O$/HCl (mL) |
|---|---|---|---|---|
| $Nb_2O_5$ | 480 | − | 100 | 0.3 ($H_2O$) |
| $Ta_2O_5$ | − | 440 | 100 | 0.3 (HCl) |
| $TaNbO_5$ | 183.2 | 275.5 | 100 | 0.3 ($H_2O$) |

## Experimental Section

**Materials.** $NbCl_5$ (99.9%) and $Ta(OC_2H_5)_5$ (99.9%) were purchased from Sigma-Aldrich. $H[(CH_2CH_2)_{0.67}(CH_2CHCH_2CH_3)_{0.33}]_{89}(OCH_2CH_2)_{79}OH$ (referred to as KLE) was used as the structure-directing agent.

**Synthesis.** In a water-free container, the inorganic precursor is combined with 2 mL of dry EtOH (0.2 mL of 37% HCl is added for $Ta_2O_5$). Once the solution is homogeneous, the KLE polymer template dissolved in a mixture of dry EtOH (3 mL) and double distilled $H_2O$ (0.3 mL) is added. Table 1 summarizes reagent masses for each type of film produced in this work. Thin films are produced via dip-coating on polar substrates including fused silica, fluorine-doped $SnO_2$ glass, and a (100)-oriented silicon wafer. Optimal conditions include 20−25% relative humidity and constant with-

(7) Ohtani, B.; Ogawa, Y.; Nishimoto, S. *J. Phys. Chem. B* **1997**, *101*, 3746–3752.
(8) Xiao, F. S. *Top. Catal.* **2005**, *35*, 9–24.
(9) Ding, Y.; Erlebacher, J. *J. Am. Chem. Soc.* **2003**, *125*, 7772–7773.
(10) Yang, P. D.; Deng, T.; Zhao, D. Y.; Feng, P. Y.; Pine, D.; Chmelka, B. F.; Whitesides, G. M.; Stucky, G. D. *Science* **1998**, *282*, 2244–2246.
(11) Sel, O.; Sallard, S.; Brezesinski, T.; Rathousky, J.; Dunphy, D. R.; Collord, A.; Smarsly, B. M. *Adv. Funct. Mater.* **2007**, *17*, 3241–3250.
(12) Sanchez, C.; Boissiere, C.; Grosso, D.; Laberty, C.; Nicole, L. *Chem. Mater.* **2008**, *20*, 682–737.
(13) Tian, B. Z.; Liu, X. Y.; Solovyov, L. A.; Liu, Z.; Yang, H. F.; Zhang, Z. D.; Xie, S. H.; Zhang, F. Q.; Tu, B.; Yu, C. Z.; Terasaki, O.; Zhao, D. Y. *J. Am. Chem. Soc.* **2004**, *126*, 865–875.
(14) Lee, J.; Orilall, M. C.; Warren, S. C.; Kamperman, M.; Disalvo, F. J.; Wiesner, U. *Nat. Mater.* **2008**, *7*, 222–228.
(15) Antonietti, M.; Niederberger, M.; Smarsly, B. *Dalton Trans.* **2008**, *1*, 18–24.
(16) Cho, K. S.; Talapin, D. V.; Gaschler, W.; Murray, C. B. *J. Am. Chem. Soc.* **2005**, *127*, 7140–7147.
(17) Baker, J. L.; Widmer-Cooper, A.; Toney, M. F.; Geissler, P. L.; Alivisatos, A. P. *Nano Lett.* **2010**, *10*, 195–201.
(18) Brezesinski, T.; Groenewolt, M.; Pinna, N.; Amenitsch, H.; Antonietti, M.; Smarsly, B. M. *Adv. Mater.* **2006**, *18*, 1827–1831.
(19) Brezesinski, T.; Wang, J.; Tolbert, S. H.; Dunn, B. *Nat. Mater.* **2010**, *9*, 146–151.
(20) Miller, J. R.; Simon, P. *Science* **2008**, *321*, 651–652.
(21) Hu, Y. S.; Adelhelm, P.; Smarsly, B. M.; Hore, S.; Antonietti, M.; Maier, J. *Adv. Funct. Mater.* **2007**, *17*, 1873–1878.
(22) Sassoye, C.; Laberty, C.; Le Khanh, H.; Cassaignon, S.; Boissiere, C.; Antonietti, M.; Sanchez, C. *Adv. Funct. Mater.* **2009**, *19*, 1922–1929.

drawal rates of 5−10 mm/s. For best results, the films are aged at 300 °C for 12 h prior to crystallization. Crystallization of the amorphous inorganic frameworks is achieved by heating films to 600 °C ($Nb_2O_5$), 750 °C ($Ta_2O_5$), and 680 °C ($TaNbO_5$) using a heating rate of 10 °C $min^{-1}$ followed by a 1 min soak.

**Methods.** Bright-field TEM images were taken with a CM30-ST microscope from Philips (acceleration voltage of 300 kV). A Philips CM200 FEG microscope with a field emission gun was used for HRTEM. FESEM images were taken with both LEO440 and LEO GEMINI 982 instruments (acceleration voltage of 5 kV). Tapping mode AFM images were collected on a multimode AFM from Vecco Instruments employing Olympus microcantilevers (resonance frequency: 300 kHz; force constant: 42 N/m). The film thickness was determined with an Alpha Step IQ Surface Profiler from KLA Tencor. 1D-WAXD measurements were carried out on a D8 diffractometer from Bruker instruments (Cu Kα radiation) equipped with an energy-dispersive solid-state detector. For 2D-WAXD, a setup with a 2D MAR image plate detector was utilized. 2D-SAXS patterns were collected on a homemade rotating anode (Nonius generator) with pinhole collimation and a MarCCD area detector (sample−detector distance: 750 mm). The use of 30 μm silicon substrates allowed SAXS measurements to be performed at arbitrary angles of incidence, $\beta$. Both surface area and porosity were determined by krypton and argon physisorption at 77 K using an automated gas adsorption station (Autosorb-1-MP) from Quantachrome Corporation. XPS spectra were acquired on a Physical Electronics ESCA 5600 spectrometer with a monochromatic Al Kα X-ray source and multichannel detector OmniIV. The electron takeoff angle to the sample surface was adjusted to 45°. The adventitious hydrocarbon C1s signal at 284.6 eV was used as the energy reference to correct for charging. The samples were also analyzed by time-of-flight secondary ion mass spectrometry using a TOF-SIMS V from ION-TOF GmbH. A beam of 25 keV $Bi^+$ focused to a 60 μm spot was used to generate secondary ions. Sputter etching was carried out using a beam of 1 keV $O^+$ ($I_O$ = 156.6 nA) focused to a 170 μm spot.

Electrochemical experiments were carried out in an argon filled glovebox in a three-electrode cell using both PAR EG&G 273 and Autolab PGSTAT302 potentiostats. A lithium foil several times the area of the working electrode was used as the counter electrode; the reference electrode was a lithium wire. The electrolyte solution was 1.0 M $LiClO_4$ in propylene carbonate (PC). Cyclic voltammetry was used to study the electrochemical behavior using cutoff voltages at 3.2 and 1.2 V vs $Li/Li^+$. For the double layer capacitance experiments, the electrolyte was changed to 1.0 M tetrabutylammonium perchlorate in PC.

## Results and Discussion

**Structure and Morphology.** The metal oxide films employed here were produced using EISA.[4] Briefly, an ethanolic solution containing both an inorganic precursor and a structure-directing agent is dip-coated onto a polar substrate. On evaporation of the solvent, the system coassembles to form an inorganic−organic composite with nanoscale periodicity. With thermal treatment this composite develops a unique pore-solid architecture with highly oriented layered nanocrystalline pore walls as described below.

In this work, we incorporated one of the poly(ethylene-*co*-butylene)-*b*-poly(ethylene oxide) diblock copolymers (referred to as KLE) as the organic template, which has already been shown to possess many desirable templating properties.[23−26]

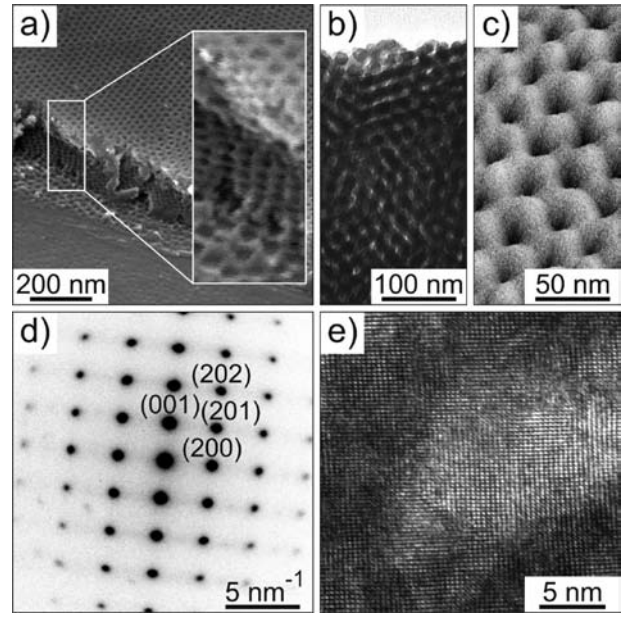


***Figure 1.*** Morphology of KLE-templated *T*-$Nb_2O_5$ films with iso-oriented nanocrystalline pore walls. (a) Cross-sectional FESEM image of a razor blade cut in a film held at a tilt of 45°. A higher-magnification image is shown in the inset of (a) confirming that the periodic structure observed on the top-surface persists throughout the film. (b) Bright-field TEM image. (c) 3D-AFM height image of the hexagonal top-surface. The contrast covers height variations in the 1−6 nm range. (d) Electron diffraction pattern obtained from the same sample shown in (b). The lattice spacings correspond well with orthorhombic $Nb_2O_5$ (*T*-phase). (e) Zone-axis HRTEM image showing that the mesopores are surrounded by iso-oriented nanocrystals.

Unlike Pluronic templates, KLE polymers are particularly suitable for the direct synthesis of ordered mesoporous oxide films with highly crystalline walls.[25,26] Part of the reason for this is the formation of an inorganic−organic composite with sufficiently thick pore walls that can be fully crystallized. In this regard, it is important to note that the same syntheses employed here failed when using Pluronic type templates, a result that further underscores the superior templating properties of KLE.

To our knowledge, this is the first work to report the soft-templating synthesis of $Ta_2O_5$ and $TaNbO_5$ solid solution thin films with both controlled nanoscale periodicity and crystallographically oriented nanocrystalline walls. Some of the group V transition metal oxides have already been prepared in powder format using various hard-templating methods, i.e., confined growth inside a rigid material.[27,28] In general, however, these approaches suffer from time-consuming processing steps and poor control of the overall homogeneity. In addition, they often involve the use of base or acid to remove the template, a treatment which can have a negative effect on material properties.

We note that the synthesis of mesoporous $Nb_2O_5$ was reported previously, and so this section will focus on extending the characterization of these materials.[18] Figure 1a and b present field-emission scanning electron microscope (FESEM) and bright-field transmission electron microscope (TEM) images of a KLE-templated $Nb_2O_5$ film after crystallization of the initially amorphous pore walls at 600 °C. These images reveal a well-

(23) Thomas, A.; Schlaad, H.; Smarsly, B.; Antonietti, M. *Langmuir* **2003**, *19*, 4455–4459.
(24) Richman, E. K.; Kang, C. B.; Brezesinski, T.; Tolbert, S. H. *Nano Lett.* **2008**, *8*, 3075–3079.
(25) Brezesinski, T.; Groenewolt, M.; Gibaud, A.; Pinna, N.; Antonietti, M.; Smarsly, B. M. *Adv. Mater.* **2006**, *18*, 2260–2263.
(26) Sallard, S.; Brezesinski, T.; Smarsly, B. M. *J. Phys. Chem. C* **2007**, *111*, 7200–7206.
(27) Kondo, J. N.; Domen, K. *Chem. Mater.* **2008**, *20*, 835–847.
(28) Nowak, I.; Jaroniec, M. *Top. Catal.* **2008**, *49*, 193–203.

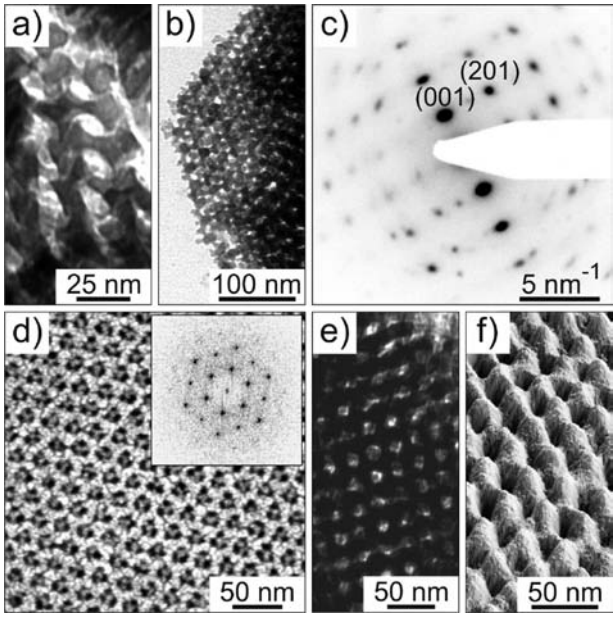


***Figure 2.*** Morphology of KLE-templated *L*-$Ta_2O_5$ (a−c) and mixed $TaNbO_5$ (d−f) films with iso-oriented nanocrystalline pore walls. (a,b) High- and low-magnification bright-field TEM images. (c) Electron diffraction pattern of a film region ∼100 nm in diameter. The presence of spots is characteristic of a system comprised of iso-oriented nanocrystals. (d) Top-view FESEM image showing open pores at the surface (sputtered with 0.5 nm of Pt). A 2D fast Fourier transform of the hexagonal top-surface is shown in the inset of (d). (e) Bright-field TEM image. (f) 3D-AFM height image.

defined cubic architecture with 13−15 nm diameter pores. They further confirm the absence of major structural defects and show the pores to be slightly deformed. This, however, is expected and can be explained by the oriented crystal growth. Moreover, it can be observed that the samples are crack-free and, more importantly, that the pores at the top-surface are open. Both the structural homogeneity and the absence of a sealing layer at the various top-surfaces are also observed with atomic force microscopy (AFM). Figures 1c, 2f, and S1 (Supporting Information) are tapping mode height and amplitude images. These micrographs show the periodic structure of the hexagonal top-surface of nanocrystalline $Nb_2O_5$ and $TaNbO_5$ samples and further underscore the flatness of these films with a root-mean-square (rms) roughness of less than 2 nm. Figure 1d is an electron diffraction (ED) pattern from a film region ∼100 nm in diameter. The presence of diffraction spots instead of Debye−Scherrer rings is characteristic of a system composed of crystalline domains where crystallographic axes are oriented relative to one another. Calculated lattice spacings are in perfect agreement with orthorhombic *T*-$Nb_2O_5$ oriented along [0*k*0]. We note that such oriented crystal growth can be achieved on virtually any substrate. In contrast, solution-processing routes (i.e., classical solution-phase epitaxy) are known to require the use of a suitable single-crystalline substrate whose lattice spacing closely matches the lattice constant of the material to be deposited. The high-resolution transmission electron microscope (HRTEM) image in Figure 1e verifies both the high crystallinity and the fact that the pores are indeed surrounded by iso-oriented nanocrystals. HRTEM also indicates the presence of lattice dislocations, which are extended over many lattice planes. This observation implies that either the nanocrystals formed during thermal treatment fuse to some extent or the presence of pores interferes with the crystallization.

Brunauer−Emmett−Teller (BET) surface area and porosity were determined by krypton and argon physisorption and by weighing several silicon substrates before and after film deposition assuming that the density of nanoscale niobia matches the solid state density of bulk *T*-$Nb_2O_5$. These measurements provide a BET surface area of ∼150 $m^2\ g^{-1}$ and a porosity of 28−31% for samples heated to annealing temperatures above 550 °C in oxygen. These values are characteristic of mesoporous materials templated with the diblock copolymer KLE.[23]

Figure 2a−f (see also Supporting Information, Figure S2) show microscopy data for $Ta_2O_5$ and $TaNbO_5$ solid solution films heated to 750 and 680 °C, respectively. Both TEM and FESEM micrographs reveal well-defined nanocrystalline architectures with ordered networks of open pores averaging 14 nm in diameter. Similar to that of *T*-$Nb_2O_5$, the samples are macroscopically homogeneous and exhibit crystallographically oriented nanocrystalline domains (Figure 2c). Together, these data indicate that KLE-templated group V transition metal oxides can be crystallized while retaining nanoscale order. Moreover, they suggest that all three systems can be readily produced with a high degree of crystallographic alignment on noncrystalline substrates by a facile solution-processing route.

The crystallization behavior, especially the oriented crystal growth, was examined in detail using wide-angle X-ray diffraction (WAXD). Figure 3a shows 1D-WAXD data obtained on mesoporous $Nb_2O_5$, $Ta_2O_5$, and $TaNbO_5$ solid solution films heated to 600, 750, and 680 °C, respectively. In addition, a 2D-WAXD pattern of a mesoporous *T*-$Nb_2O_5$ sample is shown in the inset of Figure 3a. Like electron diffraction, these data show the films to be composed of purely orthorhombic *T*-$Nb_2O_5$ and $Ta_2O_5$ (L- or $\beta$-phase), respectively, as corroborated with JCPDS (Joint Committee for Powder Diffraction Studies) reference cards #30-0873 and #25-0922. 1D-WAXD shows only one distinct peak for all three systems, namely the (1 8 0) reflection at $2\theta = 28.61°$ for *T*-$Nb_2O_5$, the (1 11 0) reflection at $2\theta = 28.45°$ for *L*-$Ta_2O_5$, and the peak at $2\theta = 28.53°$ for mixed $TaNbO_5$. The absence of other reflections (or the presence of only very weak ones) indicates pronounced crystallographic orientation relative to the plane of the substrate, perpendicular to the [1*k*0] axis of the group V transition metal oxides employed in this work. As discussed below, while all three phases are highly oriented, the $Nb_2O_5$ appears to show the best orientation as evidenced by the relative intensity of the peak at 28° compared to all other diffraction peaks.

The Warren−Averbach approach for analysis of diffraction patterns was applied to mesoporous *T*-$Nb_2O_5$ samples heated above 600 °C.[29] A nanocrystal size of 46 nm perpendicular (average maximum microstrain $\varepsilon = 0.014$) and 21 nm parallel to the substrate ($\varepsilon = 0.003$) was obtained. Taking into account the lattice parameter of the cubic architecture normal to the plane of the substrate ($a_z = 12-13$ nm, see ensuing section on SAXS), this implies that a single nanocrystal forms the wall over a distance encompassing several mesopores. The same analysis provides crystalline domain sizes of 42 and 37 nm for *L*-$Ta_2O_5$ and $TaNbO_5$, respectively, perpendicular to the substrate.

We find that the crystallization of the initially amorphous frameworks occurs within a narrow temperature interval for all three mesoporous oxides (e.g., 580−585 °C for $Nb_2O_5$). Orientation studies further reveal that the nanocrystalline domains formed at the onset of crystallization are instantly oriented with respect to the substrate and that the domain sizes

(29) Warren, B. E.; Averbach, B. L. *J. Appl. Phys.* **1950**, *21*, 595–599.

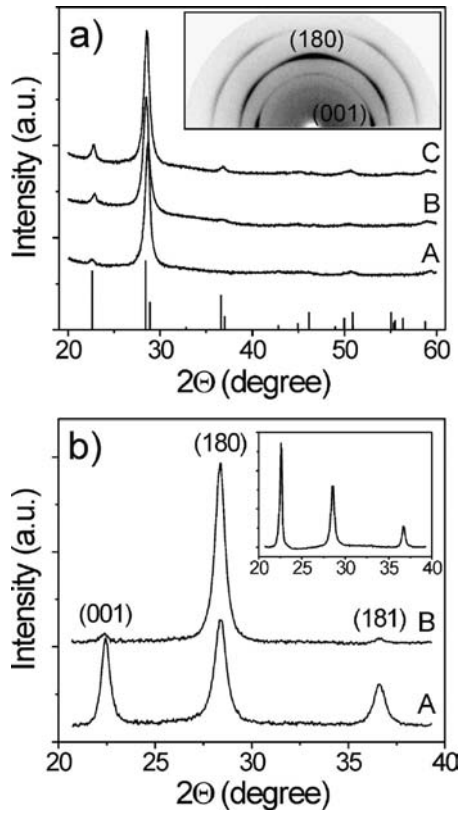


***Figure 3.*** (a) 1D-WAXD data obtained on KLE-templated *T*-$Nb_2O_5$ (A), *L*-$Ta_2O_5$ (B) and $TaNbO_5$ (C) films heated to 600, 750, and 680 °C, respectively. The stick pattern shows reference card #30-0873 for orthorhombic *T*-$Nb_2O_5$ according to JCPDS. A typical 2D-WAXD pattern for mesoporous *T*-$Nb_2O_5$ films thermally treated at 600 °C is shown in the inset of (a). (b) 1D-WAXD patterns for a mesoporous *T*-$Nb_2O_5$ sample heated to 650 °C in air. B refers to the film on a (100)-oriented silicon wafer, while A was obtained after scraping off the material from the substrate. A pattern for a nanocrystalline *T*-$Nb_2O_5$ film prepared without any KLE polymer template is shown in the inset of (b). These data verify that nontemplated versions of this material show negligible nanocrystal orientation.

mentioned above cannot be tuned. That is, the full width at half-maximum (fwhm) intensity of the diffraction peaks does not change with increasing annealing temperature up to 650 and 800 °C for *T*-$Nb_2O_5$ and *L*-$Ta_2O_5$, respectively. Treatment of films at higher temperatures, however, leads to both the loss of nanoscale periodicity and to the appearance of other reflections due to sintering effects. This behavior underscores both the excellent thermal stability of these sol−gel derived samples and the fact that both the crystallite size and orientation are fundamentally coupled to the nanoscale architecture and cannot be altered without destroying that architecture.

The crystallographic orientation results are further confirmed by 2D-WAXD measurements. The anisotropy of the diffraction pattern shown in the inset of Figure 3a gives clear evidence of the uniaxial orientation of nanocrystals relative to the substrate, while the grains are randomly oriented around an axis perpendicular to the plane of the substrate. From Figure 3a and b we are thus able to establish that a thermally induced crystallization leads to films with iso-oriented, anisotropic nanocrystals stacked on top of each other. The fact that these mesoporous materials exhibit highly oriented and, more importantly, layered nanocrystalline walls with van der Waals gaps will become important in the section on capacitive charge storage.

As discussed in the introduction, a high degree of crystallographic alignment was obtained recently for other metal oxides with a layered crystalline structure including α-$MoO_3$ (orthorhombic, #5-0508) and $V_2O_5$ (orthorhombic, #41-1426).[18,19] In contrast, oxides with lower structural anisotropy, such as $TiO_2$ (tetragonal, #21-1272) and $CeO_2$ (cubic, #34-0394), display either low or no nanocrystal orientation.[30,31] The basic requirement for this remarkable crystallographic alignment thus appears to be highly anisotropic bonding (i.e., anisotropic distribution of atoms) within the unit cell. This anisotropy typically manifests itself as a very asymmetric unit cell, such as in the case of *T*-$Nb_2O_5$ ($a = 6.175$ Å, $b = 29.175$ Å, $c = 3.93$ Å) and *L*-$Ta_2O_5$ ($a = 6.198$ Å, $b = 40.29$ Å, $c = 3.888$ Å).

While we do not yet fully understand the basis for the preferred crystallographic orientation in all of these materials, we can speculate about the cause. The layered atomic structure of both oxides leads to alternating oxygen- and metal-rich sheets normal to the long *b*-axis. These layers carry a high density of either negative or positive charges which have the potential to interact with polar surfaces. Figure S3 (Supporting Information) shows unit cells of *L*-$Ta_2O_5$ from a direction perpendicular to the long *b*-axis, which validates the layered atomic structure. Because of the coordinatively saturated nature of the atoms at the interlayer gaps, these layers also present extremely low energy surfaces which should be favored at either the substrate/sample interface or any of the many sample/air interfaces.

The question then arises as to why nontemplated versions of these materials do not show similar orientation, and there seem to be at least two possible explanations. First, we find that mesoporous versions of materials tend to crystallize at lower temperatures than their bulk counterparts. At these lower temperatures, interfacial energy may have a greater effect on crystallization kinetics. This would also explain both (1) the fact that α-$MoO_3$, which can be crystallized at temperatures below 450 °C, showed a much higher degree of crystallographic alignment (perpendicular to the [0*k*0] axis) than the group V transition metal oxides described here and (2) the finding that *T*-$Nb_2O_5$ displays a better orientation than $TaNbO_5$ and *L*-$Ta_2O_5$; the lower the crystallization temperature the better the crystallographic alignment. That is, if the thermal energy, *kT*, is too large, random grain growth will occur. Second, it is possible that that there is residual carbon between the sample and the substrate, and this carbonaceous layer may facilitate oriented nucleation in a substrate independent manner. This hypothesis is supported by the finding that only 1 wt % of KLE or other surface-active organic reagents with respect to the oxide formed is needed to achieve oriented crystal growth, while films produced without any polymer template display virtually no preferred orientation (Figure 3b, inset). Overall, it seems justified to refer to this crystallization behavior as "soft epitaxy" as the mechanism and growth mode are distinctly different from those of classical liquid phase epitaxy.

Since the details of this peculiar oriented crystallization are difficult to address by experimental means, we used modeling to provide new insights concerning this material. The procedure introduced by Segall et al. allows a "first-principles" simulation of various energy-related parameters of an atomic crystal, e.g.,

(30) Brezesinski, T.; Smarsly, B.; Groenewolt, M.; Antonietti, M.; Grosso, D.; Boissière, C.; Sanchez, C. *Stud. Surf. Sci. Catal.* **2005**, *156*, 243–248.
(31) Choi, S. Y.; Lee, B.; Carew, D. B.; Mamak, M.; Peiris, F. C.; Speakman, S.; Chopra, N.; Ozin, G. A. *Adv. Funct. Mater.* **2006**, *16*, 1732–1738.

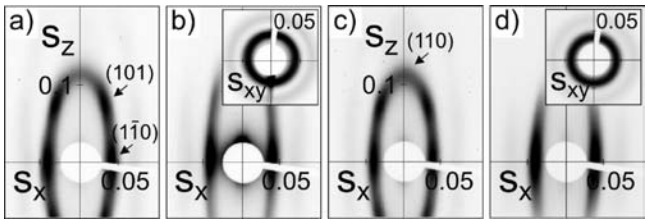


***Figure 4.*** 2D-SAXS data obtained on cubic mesoporous $Ta_2O_5$ (a,b) and $Nb_2O_5$ (c,d) thin films heated to 300 (a,c), 750 (b), and 600 °C (d). The patterns were collected at angles of incidence $\beta = 10°$ and 90° (insets) and show the evolution of the bcc pore networks upon thermal treatment. Scattering vector, *s*, components are given in 1/nm.

the morphology and the electronic polarizability in different crystallographic directions.[32] The "CASTEP" module of the molecular modeling software (Accelrys) was utilized to perform this analysis based on the corresponding CIF files as data input. This approach, however, is not applicable to *T*-$Nb_2O_5$, as to date no validated CIF file is available for this material. For α-$MoO_3$, the procedure converged and provided both the equilibrium shape and the electronic polarizability of the crystal structure. It can be seen (Supporting Information, Figure S4) that the software predicts a plate-like crystal shape which is related to the fact that the electronic polarizability is maximum parallel to the layers, i.e., perpendicular to [010]. This finding is in agreement with the crystallographic orientation obtained by the X-ray diffraction experiments. In essence, the modeling suggests that the mobility of charges is maximum perpendicular to the [010] direction and that the (0*k*0) planes are energetically most favorable. Thus, in a mechanistic scenario it seems plausible that growth of α-$MoO_3$ proceeds perpendicular to [010], i.e., with preferential orientation because electrostatic interactions are highest for these layers. The analysis of the *L*-$Ta_2O_5$ crystal structure results in a similar equilibrium crystal morphology (see Supporting Information, Figure S4), which is consistent with results and data shown in Figures 2 and 3, although the algorithm did not converge for this material. We also note that kinetic effects cannot be directly taken into account from such an analysis and instead can only be indirectly inferred from energetic considerations. Nonetheless, the calculation of the energetically favorable crystal morphology is in accordance with experimental findings.

Structural characterization of the different KLE-templated transition metal oxide films is further supported by two-dimensional small-angle X-ray scattering (2D-SAXS). Films produced on 30 $\mu$m thick silicon substrates allowed SAXS measurements to be performed at arbitrary angles of incidence, $\beta$ (defined as the angle between the X-ray beam and the plane of the substrate). Figure 4 shows 2D-SAXS data obtained on $Nb_2O_5$ and $Ta_2O_5$ thin films before and after the onset of crystallization. For small angles of incidence (here $\beta = 10°$), both materials produce patterns with distinct in-plane and off-specular maxima as well as weak out-of-plane diffraction. These maxima can be indexed to a distorted body-centered-cubic (bcc) *Im*3*m*-derived pore structure with (110) orientation relative to the plane of the substrate. We note that the presence of only weak out-of-plane maxima is due to the large incidence angle employed in these experiments. The in-plane lattice parameter, $a_x$, is in the range of 33−35 nm, which is characteristic of KLE-templated sol−gel type films. As described above, thermal treatment removes the organic template and condenses the inorganic framework, which results in a decrease in inorganic volume. On the basis of the relative position of the (110) reflection, a lattice contraction of 63−68% is determined normal to the plane of the substrate for films heated to 500 °C in air. Higher annealing temperatures do not lead to further volume change as the materials are fully cross-linked at annealing temperatures above 500 °C. Moreover, it can be observed that the samples have lost their out-of-plane periodicity after the onset of crystallization. This is due both to the small number of repeat units normal to the substrate and to the fact that the conversion of the initially amorphous pore wall structure (especially oriented crystal growth) is always accompanied by some lattice distortions.

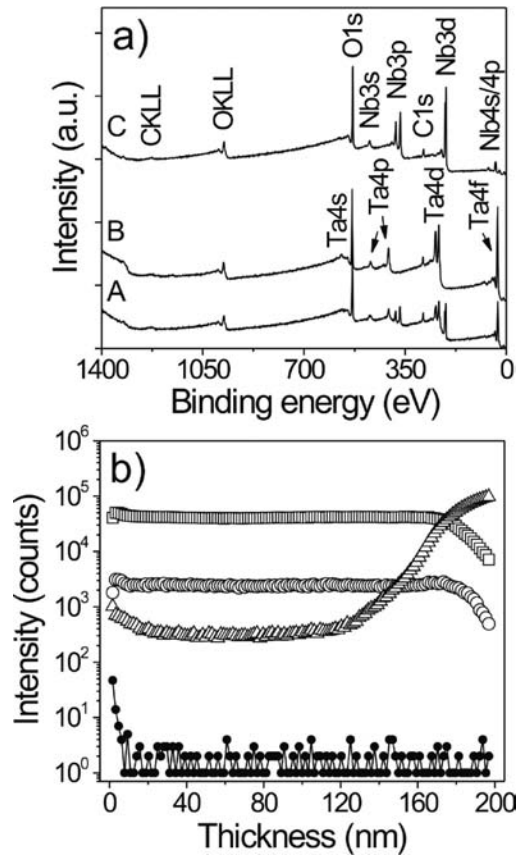


***Figure 5.*** (a) XPS survey spectra for mesoporous $TaNbO_5$ (A), *L*-$Ta_2O_5$ (B), and *T*-$Nb_2O_5$ (C) films with iso-oriented nanocrystalline pore walls. (b) TOF-SIMS sputter profile of a $TaNbO_5$ solid solution thin film on (100)-oriented silicon showing the distribution of $Nb^+$ (□), $Ta^+$ (○), $Si^+$ (△), and $C^+$ (●) as a function of depth from the surface.

2D-SAXS patterns taken in transmission mode (Figure 4, insets) reveal isotropic diffraction rings, indicating the presence of ordered polycrystalline domains even after the mesoporous frameworks have been crystallized. In conclusion, small-angle X-ray scattering demonstrates that the various cubic pore-solid architectures can be retained up to annealing temperatures as high as 650 °C ($Nb_2O_5$) and 800 °C ($Ta_2O_5$), respectively.

Lastly, a series of X-ray photoelectron spectroscopy (XPS) and time-of-flight secondary ion mass spectrometry (TOF-SIMS) measurements were carried out to determine both the chemical composition and atomic oxygen-to-metal ratio for all three systems. Figure 5a shows typical survey scans, which confirm the absence of any contaminants. Aside from very weak carbon

(32) Segall, M. D.; Lindan, P. J. D.; Probert, M. J.; Pickard, C. J.; Hasnip, P. J.; Clark, S. J.; Payne, M. C. *J. Phys.: Condens. Matter* **2002**, *14*, 2717–2744.

C1s peaks, which we associate with hydrocarbons adsorbed onto the film surface, only niobium, tantalum, and oxygen related core levels can be observed. XPS further reveals symmetric peaks (doublets due to spin orbit splitting) for the Nb3d and Ta4d regions (Supporting Information, Figure S5), the positions of which correspond well with reference data for $Nb^{5+}$ and $Ta^{5+}$. For films heated to annealing temperatures above 600 °C, the atomic oxygen-to-metal ratio is found to be 2.52 ± 0.02. The slight deviation from perfectly stoichiometric compounds can be attributed to a very small amount of extra oxygen at the film surface, presumably in the form of OH groups.

The TOF-SIMS sputter depth profile of an ~180 nm thick $TaNbO_5$ solid solution film in Figure 5b illustrates the distribution of tantalum, niobium, silicon, and carbon as a function of depth from the surface. This spectrum is in perfect agreement with XPS and shows the $TaNbO_5$ samples to be homogeneous on the atomic scale.

**Electrochemical Properties.** Transition metal oxides with layered crystalline structures are very attractive materials for charge storage because of their ability to intercalate ions in a wide range of sites.[33,34] Both faradaic and nonfaradaic mechanisms can store charge. The latter, in which charge is stored electrostatically in a thin double-layer at the electrode/electrolyte interface, is common to all materials and is not the focus here.[35,36] Rather, faradaic charge transfer mechanisms are of interest for layered oxides as three different charge storage routes are feasible when a material is immersed in an electrolyte: (1) cations react with the electroactive material which then undergoes changes to form different compositions/phases as in conventional batteries,[36,37] (2) cations electrochemically adsorb onto the surface through charge-transfer processes,[38] or (3) cations intercalate into the interlayer gaps (van der Waals gaps) of a layered material.[39] The two latter mechanisms are pseudocapacitive effects which are often referred to as redox pseudocapacitance and intercalation pseudocapacitance, respectively.[38,39] From a chemical perspective, these two are very similar in that electrochemical $Li^+$ adsorption is associated with reduction of either metal atoms located at the surface or in the interlayer lattice planes.

Previous work has shown that pseudocapacitive effects become increasingly important as metal oxides approach nanoscale dimensions.[40−42] For anatase $TiO_2$ made from preformed nanocrystalline building blocks, we showed that redox pseudocapacitance strongly benefits from a mesoporous morphology by enabling electrolyte access to the redox-active sites at the pore walls and short diffusion path lengths.[43] In addition, our recent results with α-$MoO_3$ indicated that mesoporous transition metal oxides with crystallographically oriented layered nanocrystalline walls enable another capacitive contribution to arise, that of intercalation pseudocapacitance.[19] As mentioned above, this process is associated with the insertion of $Li^+$ in the quasi-two-dimensional van der Waals gaps and was shown to occur on the same time scale as redox pseudocapacitance in molybdite (α-$MoO_3$). The result was increased charge storage without compromising charge/discharge kinetics, a very exciting development considering the potential for practical advances in electrochemical energy storage.

The significant contribution of intercalation pseudocapacitance to charge storage in mesoporous α-$MoO_3$ was related to the unique combination of (1) nanoscale porosity, which exposes the edges of the van der Waals gaps for facile $Li^+$ insertion; (2) iso-orientation of the layered nanocrystalline walls with the layers lying parallel to the plane of the substrate; and (3) mechanical (volume) flexibility, which is favorable for $Li^+$ incorporation as changes in the nanoscale structure can be used to accommodate the strain associated with intercalation processes.[19,44]

In the present work, we addressed the question of whether enhanced pseudocapacitance is unique to α-$MoO_3$ or if other iso-oriented layered nanocrystalline materials exhibit these properties. We thus decided to use the most oriented system of the group V transition metal oxides, namely *T*-$Nb_2O_5$, to test the generality of these design rules on a chemically different system.

To examine the redox processes present in KLE-templated $Nb_2O_5$, solution based voltammetry experiments were performed on films with both amorphous and crystalline wall structures. As mentioned above, we are particularly interested in determining the charging behavior at short times because one of the key advantages of electrochemical capacitors over batteries is the ability to have the faster charging. Figure 6a shows cyclic voltammograms for samples heated to 580 °C (amorphous) and 625 °C (crystalline). The amorphous films reveal a featureless voltammetric response. This type of characteristic is typical of amorphous materials and arises from the broad energy distribution of intercalation sites.[45] By contrast, the crystalline films show redox peaks (cathodic peaks at 1.75 and 1.5 V vs $Li/Li^+$ as well as a broad anodic peak at 1.8 V vs $Li/Li^+$), which have not been observed in bulk films.[46] While it is possible that these redox peaks arise from additional intercalation sites that are inaccessible to bulk materials, a more likely explanation is that the insertion/extraction kinetics for mesoporous *T*-$Nb_2O_5$ are considerably faster than that of the corresponding amorphous films.

As shown in Figure 6b, the total amount of charge stored is observed to be dependent upon charging time. Regardless of the elapsed time, however, the magnitude of stored charge for mesoporous *T*-$Nb_2O_5$ is approximately 1.6 times larger than that of the amorphous films. Since porosity, BET surface area, film thickness, and chemical composition (i.e., oxidation state, niobium-to-oxygen ratio, etc.) are basically the same for both materials, this significant difference indicates that there must be a mechanism contributing to charge storage in the mesoporous crystalline material which is not contributing to charge storage in the amorphous samples.[19] For example, at a charging

(33) Tarascon, J. M.; Armand, M. *Nature* **2001**, *414*, 359–367.
(34) Whittingham, M. S. *Chem. Rev.* **2004**, *104*, 4271–4301.
(35) Conway, B. E. *Electrochemical Supercapacitors*; Kluwer Academic: New York, 1999.
(36) Winter, M.; Brodd, R. J. *Chem. Rev.* **2004**, *104*, 4245–4269.
(37) Arico, A. S.; Bruce, P.; Scrosati, B.; Tarascon, J. M.; Van Schalkwijk, W. *Nat. Mater.* **2005**, *4*, 366–377.
(38) Conway, B. E.; Birss, V.; Wojtowicz, J. *J. Power Sources* **1997**, *66*, 1–14.
(39) Conway, B. E. *Electrochim. Acta* **1993**, *38*, 1249–1258.
(40) Jamnik, J.; Maier, J. *Phys. Chem. Chem. Phys.* **2003**, *5*, 5215–5220.
(41) Balaya, P.; Bhattacharyya, A. J.; Jamnik, J.; Zhukovskii, Y. F.; Kotomin, E. A.; Maier, J. *J. Power Sources* **2006**, *159*, 171–178.
(42) Wang, J.; Polleux, J.; Lim, J.; Dunn, B. *J. Phys. Chem. C* **2007**, *111*, 14925–14931.
(43) Brezesinski, T.; Wang, J.; Polleux, J.; Dunn, B.; Tolbert, S. H. *J. Am. Chem. Soc.* **2009**, *131*, 1802–1809.
(44) Brezesinski, T.; Wang, J.; Brezesinski, K.; Dunn, B.; Tolbert, S. H. *ACS Nano* **2010**, *4*, 967–977.
(45) Dong, W.; Mansour, A. N.; Dunn, B. *Solid State Ionics* **2001**, *144*, 31–40.
(46) Rosario, A. V.; Pereira, E. C. *J. Solid State Electrochem.* **2005**, *9*, 665–673.

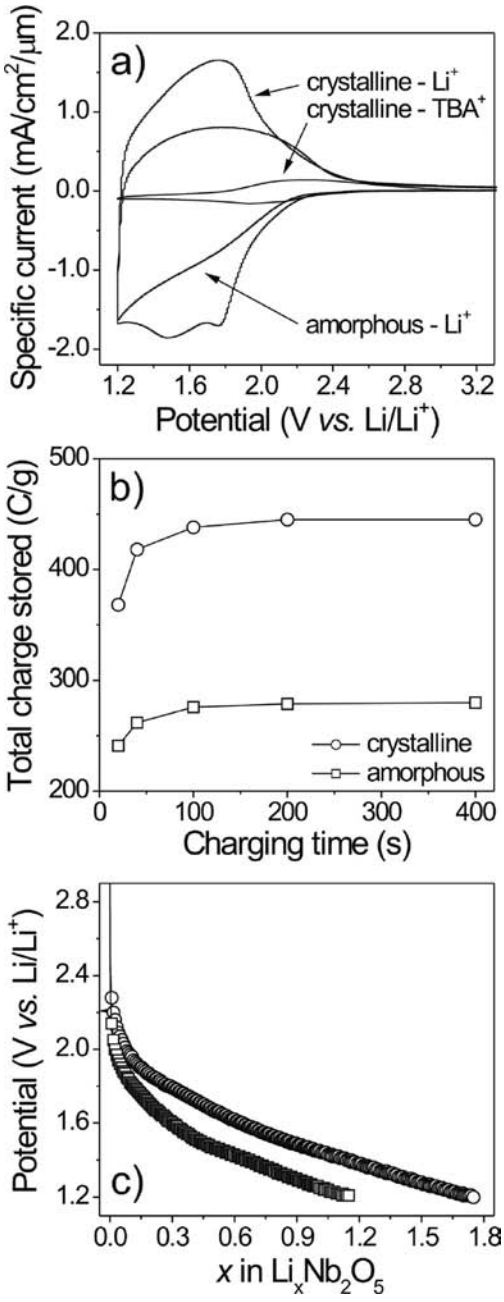


***Figure 6.*** Charge storage characteristics of mesoporous $Nb_2O_5$ films. (a) Voltammetry sweeps at a rate of 10 mV/s comparing lithium ($Li^+$) and tetrabutylammonium ($TBA^+$) electrolytes. A lower charge storage is observed with $TBA^+$ than with $Li^+$, indicating that only a minor fraction of the total charge storage stems from double layer capacitance. (b) Kinetic behavior of the various mesoporous films. The total amount of charge storage (gravimetrically normalized) as a function of charging time for *T*-$Nb_2O_5$ is much greater than that of the corresponding amorphous films. (c) Galvanostatic discharge curves at C/3 rate.

time of only 3 min, the total charge storage is 445 C/g and 280 C/g for crystalline and amorphous films, respectively.

Galvanostatic discharge curves (Figure 6c) also show the profound effect that crystallinity has on $Li^+$ intercalation, as significantly more lithium can be stored in *T*-$Nb_2O_5$ samples compared to amorphous ones. Since these experiments were carried out at a C/3 rate, charge storage arises from both capacitive and diffusion-controlled processes. Nonetheless, there are interesting features which emerge from this experiment. A closer examination of Figure 6c reveals the sloping behavior

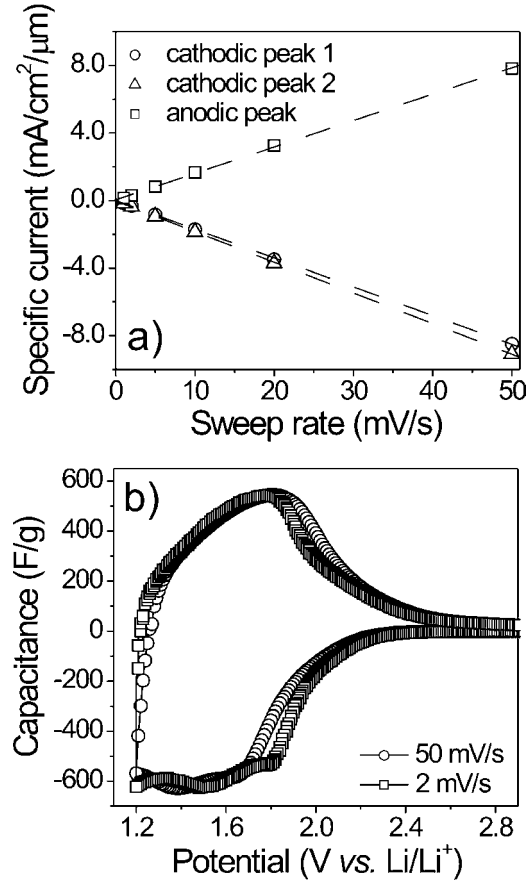


***Figure 7.*** Electrochemical characteristics of mesoporous *T*-$Nb_2O_5$ film electrodes with layered crystalline domains. (a) Specific peak current dependence on sweep rate. (b) Potential-dependent capacitance calculated from cyclic voltammetric responses at sweep rates of 2 and 50 mV/s.

of both discharge curves. This linear behavior is expected, however, as it is representative of a typical capacitive discharge.[47] The shallower slope observed for mesoporous *T*-$Nb_2O_5$ is consistent with this material having a higher capacitance. The mole fraction of stored lithium, *x*, is calculated to be 1.75 (190 mAh/g) and 1.15 (140 mAh/g) in the potential range between 3.2 and 1.2 V vs $Li/Li^+$ for the mesoporous crystalline and amorphous films, respectively. For *T*-$Nb_2O_5$, this value is close to the theoretically achievable mole fraction for a single-phase lithium intercalation process and is also higher compared to bulk films reported previously.[48,49] It is interesting to note that although both amorphous and crystalline films are insulating, there is sufficient electronic conduction to support the redox reactions associated with the lithium insertion process.

The capacitive effects were characterized by analyzing the cyclic voltammetry data assuming that the current response is proportional to the sweep rate according to

$$i = \mathrm{d}Q/\mathrm{d}t = C \cdot \mathrm{d}E/\mathrm{d}t = C \cdot v \qquad (1)$$

Here, $i$ is the current, $Q$ is the stored charge, $C$ is the capacitance, and $\mathrm{d}E/\mathrm{d}t$ is the sweep rate $v$. Figure 7a shows a

(47) Gibot, P.; Casas-Cabanas, M.; Laffont, L.; Levasseur, S.; Carlach, P.; Hamelet, S.; Tarascon, J. M.; Masquelier, C. *Nat. Mater.* **2008**, *7*, 741–747.
(48) Kumagai, N.; Koishikawa, Y.; Komaba, S.; Koshiba, N. *J. Electrochem. Soc.* **1999**, *146*, 3203–3210.
(49) Kodama, R.; Terada, Y.; Nakai, I.; Komaba, S.; Kumagai, N. *J. Electrochem. Soc.* **2006**, *153*, A583–A588.

plot of peak current versus sweep rate for mesoporous *T*-$Nb_2O_5$. The linear relationship provides key evidence that the currents arise predominantly from capacitive effects as indicated by eq 1. This result becomes particularly evident in Figure 7b, which depicts the potential dependence of the capacitance for two different sweep rates, 2 and 50 mV/s. The striking similarity between the two curves confirms the result that the total stored charge arises primarily from capacitive effects at this time scale. However, what these experiments do not tell us is whether the capacitive currents are related to double-layer or pseudocapacitive effects. This is an important question to be resolved for transition metal oxide systems if we are to take advantage of the faradaic processes occurring with these materials. Separate voltammetry experiments were thus carried out to determine the double layer capacitance by using tetrabutylammonium ($TBA^+$) perchlorate in propylene carbonate as the electrolyte. The total charge storage shown in the voltammetry sweeps in Figure 6a includes double layer capacitance, which can be easily observed using the bulky $TBA^+$, as well as pseudocapacitance and insertion processes, which are based on using $Li^+$ electrolytes. It is evident from the cyclic voltammetry data (see also Supporting Information, Figure S6) that the double layer capacitance represents only a minor contribution to the total charge storage, corresponding to ~40 C/g for both amorphous and crystalline materials.[36] The same question is also addressed in part by the fact that Figure 7b reveals broad peaks in the voltage profiles, which is characteristic of a surface-confined charge-transfer process. These results are in excellent agreement with our recent findings on α-$MoO_3$.[19]

In order to assess the influence of the iso-oriented mesoporous architecture on charge storage, we focus on the short time behavior (Figure 6b) as the charge storage processes over the first few minutes are largely capacitive. The sweep rate dependence confirms that the total charge storage for mesoporous *T*-$Nb_2O_5$ over the first few minutes of charging is virtually all capacitive, while experiments with $TBA^+$ indicate that very little of the capacitive contribution is from double layer processes. Thus, we are able to conclude that the difference in charge storage between mesoporous amorphous and crystalline $Nb_2O_5$ is from pseudocapacitive processes. While redox pseudocapacitance is expected to occur in both materials, since their mesoporous architectures and BET surface areas are the same, there is no structural reason why crystalline samples should exhibit larger values. Accordingly, we contend that mesoporous *T*-$Nb_2O_5$ enables intercalation pseudocapacitance to occur on the same time scale as redox pseudocapacitance. These results suggest that the effect of the iso-oriented nanostructure on pseudocapacitance is not limited to α-$MoO_3$ and may indeed represent a more generally observed contribution to charge storage in nanoporous versions of layered transition metal oxides.

## Conclusions

In this work, we described the self-assembly and characterization of polymer templated *T*-$Nb_2O_5$, *L*-$Ta_2O_5$, and $TaNbO_5$ solid solution films with iso-oriented layered nanocrystalline walls. The purpose of this manuscript, however, was not to be just another example of a mesoporous material. Instead, the goal was to unravel further the features of "soft epitaxy" and to validate the general design rules developed using α-$MoO_3$ as a nanoscale structural route for achieving redox and intercalation pseudocapacitance on a similar time scale in a single material.

The results with 1D- and 2D-WAXD lead us to propose that the oriented crystal growth is due in part to the layered atomic structure of the various group V transition metal oxides, which leads to alternating oxygen- and metal-rich sheets that have the potential to interact with polar surfaces. Simulations suggest that the orientation is associated with minimizing interfacial energy by oriented crystal growth along certain crystallographic directions. This anisotropy is complemented by the fact that the reduced crystallization temperatures found in these materials place more kinetic constraints on the crystallization process and may prevent simultaneous nucleation of many randomly oriented domains.

The present work further establishes the benefits of combining a mesoporous morphology with iso-oriented nanocrystalline films to achieve significant enhancement in capacitive energy storage. Redox chemistry at surface metal sites in nanoporous oxides is now well-established as a facile way to store charge that does not require $Li^+$ intercalation into the lattice and therefore slow solid-state ion diffusion and strain induced by volume expansion. Mesoporous *T*-$Nb_2O_5$ films, however, exhibit much higher charge capacities than corresponding mesoporous amorphous films of the same initial composition. This increased capacity arises from an intercalation pseudocapacitance in which the insertion of lithium ions in the interlayer gaps of *T*-$Nb_2O_5$ occurs on an extremely fast time scale (i.e., at rates comparable to traditional redox pseudocapacitance in porous $Nb_2O_5$ films).

Two factors are expected to be responsible for the facile intercalation pseudocapacitance. The nanoscale porosity provides for very short diffusion path lengths and exposes the edges of the interlayer gaps for facile $Li^+$ insertion. Perhaps more important, however, is the iso-oriented nature of the material. With the layers oriented parallel to the plane of the substrate, the entire nanoscale pore system can flex so that expansion normal to the plane of the substrate is able to accommodate the volume expansion associated with $Li^+$ insertion.[44] This unique combination of factors is likely responsible for the fast intercalation pseudocapacitance observed in these materials. From a broader perspective, these results suggest the promise of a new design paradigm for pseudocapacitive materials that exhibit both facile redox and intercalation pseudocapacitance in a single material.

**Acknowledgment.** The authors thank Thomas E. Quickel, Anneliese Heilig, Nicola Pinna, Heinz Amenitsch, Juergen Janek, and Ken-ichi Iimura for their assistance in materials preparation and measurements. This work was supported in part by the Fonds der Chemischen Industrie (T.B.). MPI of Colloids and Interfaces (Potsdam) is thanked for use of the rotating anode SAXS setup. The research at UCLA was supported in part by the Office of Naval Research and in part by the Molecularly Assembled Material Architectures for Solar Energy Production, Storage and Carbon Capture, an Energy Frontier Research Center funded by the U.S. Department of Energy, Office of Science, Office of Basic Energy Sciences under award DE-SC0001342.

**Supporting Information Available:** Low-magnification FESEM and AFM images. High-resolution XPS spectra. Schematics of equilibrium morphologies and unit cells. Cyclic voltammetry data. This material is available free of charge via the Internet at http://pubs.acs.org.

JA9106385